Tradeoff Between Speed and Robustness in Primordium Initiation Mediated by Auxin-CUC1 Interaction

Shuyao Kong,[1,2] Mingyuan Zhu,[1,2,3] David Pan,[1,2] Brendan Lane,[4] Richard S. Smith,[4] Adrienne H. K. Roeder[1,2,5,*]

[1] Weill Institute for Cell and Molecular Biology, Cornell University, Ithaca, NY 14853, USA

[2] Section of Plant Biology, School of Integrative Plant Science, Cornell University, Ithaca, NY 14853, USA

[3] Present address: Department of Biology, Duke University, Durham, NC 27708, USA

[4] Department of Computational and Systems Biology, John Innes Centre, Norwich NR4 7UH, UK.

[5] Lead Contact

[*] Correspondence: ahr75@cornell.edu

ABSTRACT

Robustness is the reproducible development of a phenotype despite stochastic noise. It often involves tradeoffs with other performance metrics, but the mechanisms underlying such tradeoffs were largely unknown. An *Arabidopsis* flower robustly develops four sepals from four precisely positioned auxin maxima. The *development related myb-like 1* (*drmy1)* mutant generates stochastic noise in auxin signaling that disrupts both the robust position and number of sepal primordia. Here, we found that increased expression of *CUP-SHAPED COTYLEDON1* (*CUC1*), a boundary specification transcription factor, in the *drmy1* mutant underlies this loss of robustness. CUC1 surrounds and amplifies stochastic auxin patches in *drmy1* to form variably positioned auxin maxima and sepal primordia. Removing *CUC1* from *drmy1* provides time for the noise in auxin signaling to resolve into four precisely positioned auxin maxima, restoring robust sepal initiation. However, removing CUC1 decreases auxin maxima intensity and slows down sepal initiation. Thus, CUC1 increases morphogenesis speed but impairs robustness against auxin noise. Further, using a computational model, we found that the observed phenotype can be explained by the effect of CUC1 in repolarizing PIN FORMED1 (PIN1), a polar auxin transporter. Thus, our study illustrates a tradeoff between speed and robustness during development.

Keywords: Robustness, tradeoff, primordium initiation, sepal, Arabidopsis, auxin, CUC1

INTRODUCTION

Cells within an organism experience a multitude of noise, such as stochastic gene expression[1] and heterogenous growth rate[2,3]. Despite such noise, organisms often develop invariantly and reproducibly, a phenomenon termed developmental robustness[4]. How developmental robustness is achieved is one of the most intriguing open questions in cell biology[5], which has attracted increasing research efforts in recent years[2,3,6–18]. It was shown that noise in morphogen signaling can be buffered by certain gene regulatory network structures[13,14] and self-organized cell sorting[11,15] to achieve robust patterning. Noise in growth rate can be buffered by averaging growth among neighboring cells[2,3] or in the same cell over time[2] to achieve robust organ size and shape. Notably, robustness is often involved in tradeoffs with other important aspects of development[19–21]. For example, during porcine embryogenesis, manual removal of zona pellucida speeds up development by a few hours but significantly reduces the robustness of blastocysts development in terms of symmetry and cell size uniformity[21]. How such tradeoffs are mediated remains largely unknown.

In plants, developmental robustness has been studied in sepals[2,3,16–18,22]. Sepals are the outermost floral organs that enclose and protect the immature bud before the flower opens. To achieve this protection, each flower robustly develops four sepals of constant size, positioned evenly around the bud typical of a cruciferous flower. This robustness in size, number, and position ensures tight closure critical for protection (Fig. 1a). In contrast, the *development related myb-like 1* (*drmy1*) mutant produces 3-5 sepals of different sizes, unevenly positioned, leaving gaps that expose the inner floral organs (Fig. 1a)[16,17]. This loss of developmental robustness originates during the initiation of sepals from the floral meristem, where the sepal primordia are robust in size, number, and position in wild type (WT) but variable in *drmy1* (Fig. 1b)[16]. We have been studying how DRMY1 maintains robust sepal development. We previously showed that DRMY1 maintains robustness by increasing TARGET OF RAPAMYCIN (TOR) signaling and protein translation, which supports the rapid synthesis of A-type ARABIDOPSIS RESPONSE

59 REGULATOR (ARR) proteins to dampen cytokinin signaling. A proper level of cytokinin signaling
60 ensures robust patterning of auxin signaling and sepal initiation. In *drmy1*, lack of A-type ARR
61 proteins and the consequent upregulation of cytokinin signaling increases stochastic noise in
62 auxin patterning, underlying variable sepal initiation[17]. However, whether there are any tradeoffs
63 between robustness and other properties of development in this system remains unknown.

64 Here, we found that a tradeoff exists between robustness and speed of sepal initiation
65 from the floral meristem. In WT, strong, robust auxin maxima restricts the expression of *CUP-*
66 *SHAPED COTYLEDON1* (*CUC1*), encoding a boundary-specifying transcription factor[23,24], to
67 precise boundary domains immediately outside the auxin maxima. CUC1 increases the intensity
68 of auxin maxima it surrounds, and promotes rapid sepal initiation. In *drmy1*, lack of robustness in
69 auxin patterning causes an expansion of *CUC1* expression. CUC1 amplifies stochastic auxin
70 noise in the *drmy1* floral meristem, forming variably positioned auxin maxima and sepal primordia.
71 Removing CUC1 slows down sepal initiation but provides robustness against noise. Thus, the
72 feedback interactions between auxin and CUC1 promotes rapid organogenesis under low noise
73 conditions, but disrupts robustness under high noise conditions. Our study thus illuminates the
74 mechanism behind the tradeoff between robustness and speed during organ initiation.

75

76 **RESULTS**

77 ***CUC1* is upregulated in *drmy1* mutant**

78 To gain insights into key mechanisms controlling developmental robustness, we
79 previously performed RNA-seq on inflorescence tissue of *drmy1* vs. WT at the stage of sepal
80 primordium initiation[17]. We found a 2.4-fold increase in the expression of *CUC1* in *drmy1*, but not
81 for its paralogs *CUC2* and *CUC3* (Fig. 1c). *CUC* genes encode NAC (NAM, ATAF1,2, CUC2)
82 family transcription factors important for boundary specification[23,24]. To investigate where *CUC1*
83 is upregulated within the floral meristem, we imaged the *CUC1* transcriptional reporter. In WT,
84 *CUC1* is expressed in four precisely specified boundaries separating the incipient sepal primordia

85 from the center of floral meristem and each other, first appearing in the lateral boundaries followed
86 by the outer and inner boundaries (Fig. 1d). In contrast, in *drmy1*, *CUC1* expression is expanded
87 and localized to the bud periphery in early stage 2 meristems (Fig. 1e, Supplementary Movie 1).
88 As the bud develops, this broadened expression coalesces into narrower, WT-like boundary
89 domains in some parts of the bud (Fig. 1e, arrowheads), but remains in the bud periphery in other
90 parts (Fig. 1e, brackets), correlated with the presence or absence of sepal outgrowth in stage 3.
91 *drmy1* shows a similar disruption in the protein accumulation pattern of CUC1 (Fig. 1f, g,
92 Supplementary Movie 2), as well as the expression and protein accumulation patterns of CUC2
93 (Supplementary Fig. 1).

94 It was previously shown that auxin inhibits the expression of *CUC* genes and restricts them
95 to organ boundaries[25–27]. In the WT floral meristem, CUC1 accumulates in four boundaries
96 immediately outside the four auxin maxima (Supplementary Fig. 2a). In *drmy1*, diffuse, bud
97 periphery-localized CUC1 colocalizes with diffuse, weak bands of auxin signaling. As these auxin
98 bands concentrate into variably positioned auxin maxima, CUC1 domains retreat from the bud
99 periphery and refine into boundaries around the auxin maxima (Supplementary Fig. 2b). These
100 observations led us to hypothesize that the broadened *CUC1* expression in *drmy1* is due to lack
101 of robust, concentrated auxin maxima. Consistent with this idea, buds treated with L-Kynurenine
102 (L-Kyn, inhibitor of auxin synthesis) or Naphthylphthalamic acid (NPA, inhibitor of polar auxin
103 transport), both of which reduce auxin maxima (Supplementary Fig. 2c, d), show an expansion of
104 *CUC1* expression into the bud periphery (Supplementary Fig. 2e, f). Treatment with both 1-
105 Naphthaleneacetic acid (NAA) and NPA, which uniformly increases auxin signaling around the
106 bud periphery (Supplementary Fig. 2d), largely represses *CUC1* expression, and only a weak ring
107 of *CUC1* expression immediately inside the bud periphery remains (Supplementary Fig. 2f).
108 These results support the idea that robust, concentrated auxin maxima are required for the
109 precise boundary expression of *CUC1*, and that *drmy1* shows expanded *CUC1* expression due
110 to diffuse auxin signaling.

111

112 ***CUC1* upregulation is necessary and sufficient for variable sepal initiation**

113 We next tested the phenotypic consequence of *CUC1* upregulation, by imaging plants in
114 which the repression of *CUC1* by miR164[28–30] has been removed. Specifically, we imaged *miR164*
115 mutants (*eep1*[30], *mir164abc*[29]), and plants carrying *CUC1* expression constructs in which the
116 miR164 target sequence has been mutated (*5mCUC1*[28] and *CUC1m-GFP*[30]). In WT, buds
117 robustly develop four sepal primordia that are evenly spaced (Fig. 1b, 2a)[16,17]. We found that this
118 robustness is disrupted in buds upregulating *CUC1*, which, similar to *drmy1*, produce a range of
119 2-6 sepal primordia that are unevenly spaced and of different sizes (Fig. 2b-e, Supplementary
120 Fig. 3a-h). In WT, uniform sepal size within each flower is achieved by coordinated initiation timing
121 between sepal primordia, where inner and lateral sepals initiate within 12 hours of the outer sepal
122 (Supplementary Fig. 4a, c)[16]. In contrast, in *drmy1*, variability of sepal size originates from the
123 disorganized initiation timing, where the initiation of the inner and lateral sepals are severely
124 delayed (Supplementary Fig. 4f, h)[16]. Similar to *drmy1*, we found that in buds upregulating *CUC1*,
125 the initiation of inner and lateral sepals are greatly delayed relative to the outer sepal, underlying
126 the variability in size (Supplementary Fig. 4a-c). In addition, the time difference between outer,
127 inner, and lateral sepal initiation events is more variable between buds (Supplementary Fig. 4c).
128 Overall, these results suggest that *CUC1* overexpression is sufficient to disrupt the robustness in
129 number, position, and coordinated initiation timing of sepal primordia.

130 Our results show that *CUC1* overexpression is sufficient for disrupting robustness in sepal
131 initiation, but is it also necessary? We found that the *drmy1 cuc1* double mutant often robustly
132 develops four sepal primordia that are evenly spaced, rescuing the variability in sepal number
133 and position in *drmy1* (Fig. 2f-k). The result is specific to *cuc1* since the *drmy1 cuc2* double mutant
134 exhibits disrupted robustness similar to *drmy1* (Supplementary Fig. 3i-n). While the *cuc1* mutation
135 restores robustness in sepal primordia number and position in *drmy1*, it does not restore
136 robustness in sepal primordia size and coordination of initiation timing (Supplementary Fig. 4d-

137 h), suggesting that other mechanisms also contribute to these defects. Overall, these results show
138 that *CUC1* upregulation causes the variability of sepal primordium number and position in *drmy1*.
139

140 **CUC1 increases auxin maxima intensity and facilitates rapid sepal initiation**

141 CUC1 functions redundantly with CUC2 and CUC3 in organ separation[31,32], and the *cuc1*
142 *cuc2* double mutant shows sepal fusion in stage 8 flowers[31]. However, *cuc1 cuc2* flowers robustly
143 initiate four sepal primordia at stage 4, suggesting that they are dispensable for sepal initiation.
144 Then why is *CUC1* still expressed so early on in the floral meristem, when it has the potential to
145 disrupt robustness when dysregulated (Fig. 2)? Comparing buds of similar size (as an indicator
146 of similar developmental progression), we found that overexpression of *CUC1* makes the outer
147 sepal primordium initiate earlier from the floral meristem (Fig. 3a-c). This increased speed in outer
148 sepal initiation correlated with an increase in auxin signaling (Fig. 4a, b). Mutation of *CUC1* delays
149 the initiation of all four sepals relative to bud size (Fig. 3d-f), correlated with weaker auxin signaling
150 maxima (Fig. 4a, b). These results suggest that CUC1 increases auxin maxima intensity, which
151 in turn promotes rapid sepal initiation to promptly cover and protect the developing floral meristem.
152 This beneficial role may explain why *CUC1* is expressed in the early-stage floral meristem despite
153 its potential in reducing developmental robustness when dysregulated, and suggests a potential
154 conflict between speed and robustness in sepal initiation.
155

156 **CUC1 amplifies sporadic auxin noise into variably positioned auxin maxima**

157 How does *CUC1* mislocalization disrupt developmental robustness in *drmy1*? There is
158 evidence that feedback interaction between CUC and auxin plays an important role in plant
159 morphogenesis[25], and we previously showed that the disrupted pattern of auxin signaling
160 underlies variable sepal initiation in *drmy1*[16]. Our results illustrated the first half of the feedback
161 loop where auxin regulates CUC1, by showing that diffuse auxin signaling underlies the
162 mislocalization of CUC1 expression in *drmy1* (Supplementary Fig. 2). Here, we hypothesized the

second half of the feedback loop where CUC1 regulates auxin, and tested whether CUC1 mislocalization disrupts robustness in auxin pattern in *drmy1*. In WT, four auxin maxima form robustly, marking four incipient sepal primordia (Fig. 4a, Outer, Inner, Lateral, Lateral). We found that this robustness is disrupted in *5mCUC1* (CUC1 overexpression), as additional auxin maxima form (Fig. 4a, arrow). The *cuc1* single mutant forms four auxin maxima robustly, although weaker (Fig. 4a, b). The *drmy1* single mutant, where CUC1 is upregulated and mislocalized, shows diffuse, noisy bands of auxin signaling (Fig. 4a, brackets). Removing CUC1 from *drmy1* restores four robustly positioned auxin maxima (Fig. 4a, c-d). Overall, these results are consistent with the second half of the feedback loop where CUC1 mislocalization disrupts robustness in auxin pattern.

How is robust auxin pattern disrupted when *CUC1* is upregulated, and restored when *CUC1* is removed? To address this question, we live imaged buds of WT, *5mCUC1*, *cuc1*, *drmy1*, and *drmy1 cuc1* every 6 hours from late stage 1 to early stage 3 (Fig. 4e-n). Initially, WT buds show three robustly positioned auxin maxima. One of them is in the cryptic bract (a suppressed inflorescence leaf), a remnant of floral meristem initiation[33–36]. The other two auxin maxima appear in the incipient lateral sepals. These auxin maxima are later followed by two more in the incipient outer and inner sepals (Fig. 4e, j, Supplementary Movie 3). In *5mCUC1*, some buds initially form WT-like pattern of four auxin maxima, followed by additional ones in between (Fig. 4f, k, arrows, Supplementary Movie 4). Other buds display more dynamic spatiotemporal changes in auxin maxima localization (Supplementary Fig. 5). This suggests that *CUC1* overexpression disrupts auxin patterning by inducing the formation of new auxin maxima and making them more dynamic. In *cuc1*, auxin maxima sequentially and robustly form like in WT, although weaker (Fig. 4g, l, Supplementary Movie 5). In *drmy1*, auxin signaling initially appears as diffuse, noisy bands with sporadic patches of cells having stronger signal than neighboring cells which fluctuates over time (Fig. 4h, m, brackets). These sporadic patches seed the subsequent formation of variably sized and positioned auxin maxima (Fig. 4h, m, arrowheads). As the bud further expands, additional

189 auxin maxima form, similar to *5mCUC1* (Fig. 4h, m, arrows, Supplementary Movie 6). In *drmy1*
190 *cuc1*, auxin signaling initially accumulates in sporadic patches, but unlike *drmy1*, they fade away,
191 allowing the subsequent formation of the robust auxin pattern (Fig. 4i, n, asterisk, Supplementary
192 Movie 7). Our results suggest that increased *CUC1* expression disrupts robust auxin patterning
193 in *drmy1* by amplifying sporadic auxin noise to form variably positioned auxin maxima.

194 We next tested whether CUC1 amplifies sporadic auxin noise from sources other than the
195 *drmy1* mutation. It was previously shown that exogenous cytokinin alters patterns of polar auxin
196 transport[37,38], causing sporadic patches of PIN convergence and auxin signaling[16]. We
197 hypothesized that the cytokinin induced sporadic patches of auxin signaling would not be
198 amplified in the *cuc1* mutant, and over-amplified in *CUC1* overexpression (*5mCUC1*) buds.
199 Indeed, WT buds treated with the synthetic cytokinin 6-Benzylaminopurine (BAP) amplifies
200 sporadic auxin patches to form variably positioned auxin maxima and sepal primordia (Fig. 5a, b,
201 g-k). While BAP induces sporadic auxin noise in early stage 2 buds of *cuc1*, it quickly fades away,
202 and most buds robustly form four sepal primordia (Fig. 5c, d, g-k). In contrast, *5mCUC1* buds
203 treated with BAP form numerous auxin maxima that often connect into a ring, which grow into 3-
204 8 primordia, more variable than the mock-treated, and often with mixed sepal-petal identity (Fig.
205 5e-k). Overall, these data support the idea that, under conditions that increase noise in auxin
206 patterning, such as *drmy1* or under exogenous cytokinin treatment, CUC1 amplifies the noise to
207 form variably positioned auxin maxima, which in turn disrupts robustness in sepal initiation. In the
208 absence of CUC1, these noisy patches are not amplified and quickly fade away, leaving four
209 robust auxin maxima.

210

211 **Modeling predicts CUC1 amplifies auxin noise by repolarizing PIN**

212 It was previously reported that *CUC* genes promote PIN polarity[25,39]. We wondered
213 whether an increase in PIN repolarization could explain the noise-amplifying effect of *CUC1*. To
214 test this, we implemented a computational model of auxin pattern formation (Supplementary

215 Dataset 2). The floral meristem was modeled using a 2D growing disk of cells, where cells divide
216 when a size threshold is met. In each cell, PIN1 transports auxin to neighboring cells with highest
217 auxin concentration. This up-the-gradient auxin transport has been shown to generate auxin
218 maxima patterns from a homogeneous initial condition with small perturbations[40–42] and is a
219 potential mechanism of auxin noise amplification. CUC1 is produced in cells with low auxin
220 concentration. The sole function of CUC1 in the model is to increase PIN repolarization. Below a
221 CUC1 concentration threshold, PIN repolarizes linearly according to the auxin concentration of
222 neighboring cells; above the threshold, PIN repolarizes quadratically, and is thus more sensitive
223 to auxin concentration differences among neighboring cells (Fig. 6a). We hypothesize that this
224 function of CUC1 in increasing PIN repolarization can by itself promote auxin maxima formation
225 while amplifying auxin noise. Starting with a patternless disk of cells with small fluctuations in
226 auxin production rate, auxin maxima form, which are then extracted and quantified (Fig. 6b). We
227 modeled the *drmy1* mutation by increasing the amplitude of fluctuation in auxin production rate,
228 which recreates the sporadic auxin patches and PIN convergence points observed in *drmy1*[16]
229 (Fig. 6c). We modeled the *cuc1* mutant by eliminating CUC1 production (Fig. 6c). We found that
230 in both WT and *drmy1* models, having CUC1 results in stronger, more concentrated auxin maxima
231 that form more rapidly compared to *cuc1* and *drmy1 cuc1* respectively (Fig. 6d-h). These modeling
232 results are similar to real buds (Fig. 4a, b). In both the model and the data, while *drmy1* amplifies
233 auxin production noise, creating variability in the final auxin pattern (Fig. 6f, arrowheads), *drmy1*
234 *cuc1* shows a relatively robust final pattern despite initial noise (Fig. 6g, arrows, 6i, Supplementary
235 Movie 8). These simulations suggest that the previously demonstrated function of CUC1 in
236 increasing PIN repolarization is sufficient for its role in promoting rapid, strong auxin maxima
237 formation while disrupting robustness against high auxin noise.

238 In addition to an increase in PIN repolarization which transports more auxin up the
239 concentration gradient, noise may also be amplified if a cell rapidly grows and divides, forming
240 two daughter cells that inherit the same auxin noise, before noise is dampened by transport or

241 decay (Supplementary Fig. 6a). To test this idea, we examined the effects of tissue growth rate
242 (which correlates with cell division rate in the model) on robustness of auxin patterning. We found
243 that increasing growth rate increases variability of auxin maxima in both WT and *drmy1*, while
244 reducing growth rate restores robust auxin patterning in *drmy1* (Supplementary Fig. 6b, d). In
245 *drmy1* simulations under reduced growth rate, the initial stochastic noise in auxin concentration
246 fades, allowing the formation of robust auxin pattern (Supplementary Fig. 6c), similar to
247 simulations of the *drmy1 cuc1* double mutant (Fig. 6g). This finding supports the idea that speed
248 and robustness can be conflicting sides of pattern formation during development.

249 It was previously shown that spatiotemporal averaging of cell heterogeneity can underlie
250 tissue-wide developmental robustness[2,43,44]. We hypothesize that reduced PIN sensitivity to
251 fluctuating auxin levels in neighboring cells (Fig. 6g) or reduced growth rate (Supplementary Fig.
252 6b, c) restores robust auxin patterning because they allow more time for auxin noise to average
253 to concentrations similar to nearby cells. We deduce that setting auxin noise temporally (but not
254 spatially) unchanging would eliminate this averaging (Supplementary Fig. 7a), and thus mutating
255 *cuc1* or reducing growth rate would no longer rescue the *drmy1* patterning defect. Indeed, when
256 noise is set temporally unchanging, both *drmy1* and *drmy1 cuc1* shows stabilization of initial auxin
257 noise into variably positioned auxin maxima, as does *drmy1* under reduced growth rate
258 (Supplementary Fig. 7b-d). Overall, these results support our idea that increased CUC1 disrupts
259 robustness in auxin patterning by increasing the sensitivity of PIN to fluctuating auxin levels, which
260 hinders temporal noise averaging and promotes noise amplification.

261

262 **DISCUSSION**

263 Developmental robustness has fascinated biologists for over 80 years[45], yet the underlying
264 mechanisms have just begun to be explored[2–4,6–18]. Here, we elucidated a mechanism through
265 which the developmental robustness of sepals is shaped by DRMY1-auxin-CUC1 interaction (Fig.
266 6j). In the floral meristem, DRMY1 maintains robust auxin patterning[16] which in turn restricts the

expression of *CUC1* to precise boundary domains adjacent to auxin maxima (Fig. 1d, f, Supplementary Fig. 2). CUC1 increases the intensity of auxin maxima and promotes rapid sepal initiation (Fig. 3, 4a, b). In the *drmy1* mutant, diffuse, noisy auxin signaling causes an upregulation and expansion of the *CUC1* expression domain (Fig. 1e, g, Supplementary Fig. 2). CUC1 amplifies sporadic auxin patches to form variably positioned auxin maxima and sepal primordia (Fig. 4, 5). In the *drmy1 cuc1* double mutant, auxin fluctuations have time to average out, allowing robust auxin pattern formation (Fig. 6, Supplementary Fig. 7) and robust sepal initiation (Fig. 2).

In an Arabidopsis flower, sepals enclose and protect the inner, developing floral organs before the flower opens. To achieve this function, they need to not only rapidly initiate from the floral meristem to promptly cover it, but also develop robustly so as to not leave any gaps (Fig. 1a). We found that these two traits, speed and robustness, are conflicting sides of sepal development, and that this tradeoff is mediated by auxin-CUC1 interaction. CUC1 promotes strong auxin maxima formation and rapid sepal initiation, but also stabilizes auxin noise and can therefore disrupt robustness under high auxin noise (Fig. 6j, left). On the other hand, lack of CUC1 slows down sepal development, but also allows time for noisy auxin signaling to robustly converge (Fig. 6j, right).

Our computational modeling suggest that this speed-robustness tradeoff can be fully explained by the previously reported function of CUCs in increasing PIN polarity[25,39]. How CUCs increase PIN polarity remains unknown. It was shown that PIN polarity can be regulated by phosphorylation (e.g., PID[46], D6PK[47], and PP2A[48]) or membrane trafficking (e.g., ABCB19[49] and ROP2[50]). Thus, CUCs may increase PIN polarity by changing the expression of these important PIN regulators. Alternatively, CUCs may also inhibit growth, causing mechanical conflict with adjacent fast-growing regions which alters PIN polarity[51]. Further study is needed to test whether CUCs increase PIN polarity by any of these mechanisms.

Is morphogenesis speed always involved in a tradeoff with robustness? Can a system achieve both aspects simultaneously? Earlier theoretical studies on the mammalian olfactory

293 epithelium suggest that tissue regeneration regulated by a feedback loop cannot achieve both
294 speed and robustness, unless a second feedback loop is involved[19,20]. Similarly, a recent study
295 on Hedgehog signaling shows that coupled extracellular and intracellular feedback loops
296 mediated by PTCH provides both robustness and speed of signaling gradient formation,
297 compared to single or uncoupled feedback loops[13]. In summary, at the cost of additional
298 regulatory mechanisms, morphogenesis speed and robustness may be both achieved
299 simultaneously.

300 **MATERIALS AND METHODS**

301 **Plant material**

302 Most Arabidopsis plants were in Col-0 background (WT). Plants presented in
303 Supplementary Fig. 1, 3a-c, 3e-f, and 7e were in Ler background. *mir164abc* was in a mixed Ler-
304 Col background[29]. *drmy1* (Ler) was generated by backcrossing *drmy1* (Col-0) with Ler twice. The
305 following lines were provided by the Arabidopsis Biological Resource Center: *pCUC2::3xVENUS-*
306 *N7* (CS23891)[52], *pCUC2::CUC2-VENUS pPIN1::PIN1-GFP* (CS67929)[52], *pCUC1::CUC1m-GFP*
307 (CS65830)[30], *cuc1-13* (SALK_006496C), *cuc2-3* (CS875298), *eep1* (CS65826)[30], and *mir164a-4*
308 *mir164b-1 mir164c-1* (CS65828)[29]. In addition, the following lines were previously described:
309 *drmy1-2*[16], *5mCUC1*[28], *pCUC1::3xVENUS-N7*[29], *pCUC1::CUC1-GFP*[53], *DR5rev::3xVENUS-N7*[52],
310 *DR5rev::ER-mRFP1.2*[54], *35S::mCitrine-RCI2A*[16]. *pCUC1::3xVENUS-N7* in Col-0 background
311 (Fig. 1d-e) was generated by transforming Col-0 plants with the *pCUC1::3xVENUS-N7* construct.
312

313 **Plant growth conditions**

314 Seeds were sown in wetted Lambert LM-111 soil and stratified at 4°C for 3-5 days. Plants
315 were grown under 16 h – 8 h light-dark cycles (fluorescent light, 100 µmol m^{-1} s^{-1}) at 22°C in a
316 Percival walk-in growth chamber.
317

318 **Flower staging**

319 Flower buds were staged as previously described[55].
320

321 **Confocal microscopy**

322 Confocal imaging was done as previously described[16,17]. Briefly, inflorescences were cut
323 and dissected with a Dumont tweezer (Electron Microscopy Sciences, style 5, no. 72701-D) down
324 to stage 9, inserted upright into a small petri dish (VWR, 60 x 15 mm) containing inflorescence
325 culture medium (1/2 MS, 1% (w/v) sucrose, 1x Gamborg vitamin mixture, 0.1% (v/v) plant

326 preservative mixture (Plant Cell Technology), 1% (w/v) agarose, pH 5.8), further dissected down
327 to stage 6 (for static imaging) or stage 2 (for live imaging), immersed with water, and imaged
328 under a Zeiss710 upright confocal microscope with a 20x Plan-Apochromat water-dipping lens
329 (1.0 NA). For static imaging, to visualize tissue morphology, samples were stained with 0.1 mg/ml
330 propidium iodide (PI) for 5 minutes before imaging. For live imaging, dissected samples were put
331 in a 24 h-light growth chamber (fluorescent light, 100 μmol m^{-1} s^{-1}) between time points. To prevent
332 bacterial growth, every 2-3 days, samples were transferred onto fresh media and treated with 100
333 μg/ml Carbenicillin (GoldBio, C-103-5, lot # 0129.091814A).

334 The following lasers and wavelengths were used. Chlorophyll, excitation 488 or 514 nm,
335 emission 660-722 nm (when also imaging mRFP1.2) or 647-721 nm (others). Propidium iodide,
336 excitation 514 nm, emission 590-660 nm. mRFP1.2, excitation 561 nm, emission 582-657 nm.
337 mCitrine, excitation 514 nm, emission 519-580 nm. For VENUS, in *DR5::3xVENUS-N7* and
338 *pCUC2::CUC2-VENUS*, excitation 514 nm, emission 519-558 nm; in *pCUC1::3xVENUS-N7*,
339 excitation 514 nm, emission 518-578 nm; in *pCUC2::3xVENUS-N7*, excitation 488 nm, emission
340 493-550 nm. GFP, excitation 488 nm, emission 493-556 nm.

341

342 **Image processing**

343 Image processing was done as previously described[16,17] and also briefly described below.

344 Tissue morphology was visualized by taking screenshots of the Chlorophyll, PI, or
345 *35S::mCitrine-RCI2A* channels in MorphoGraphX[56] or by 3D rendering in the ZEN software
346 (Processing → 3D). For Fig. 3 and Supplementary Fig. 4, to aid visualization of sepal initiation,
347 Gaussian curvature heatmaps were calculated in MorphoGraphX as follows: Gaussian blur (X/Y/Z
348 sigma = 1 μm twice and then X/Y/Z sigma = 2 μm once), edge detection (threshold = 2000-8000
349 depending on brightness, multiplier = 2.0, adapt factor = 0.3, fill value = 30000), marching cube
350 surface (cube size = 8 μm, threshold = 20000), change lookup table to “jet”, subdivide mesh,
351 smooth mesh (passes = 5), subdivide mesh, smooth mesh (passes = 5), and project mesh

curvature (type = Gaussian, neighborhood = 10 μm, autoscale = no, min curv = -0.002, max curv = 0.002). A sepal primordium is considered initiated when it emerges as a deep red band (positive curvature) separated from the floral meristem by a deep blue band (negative curvature).

For circular histograms and kymographs of DR5 signal, each stack was cropped in ImageJ and trimmed using the Voxel Edit function in MorphographX[56] so that only the focal bud remained in the stack. The bud was positioned so that it was centered, facing the Z direction, and the incipient outer sepal was at 45°. A circular histogram was calculated using the function Export Histogram Circular, summing signal (in voxel intensity units, 0-255) in each 1° sector around the Z axis starting from 0° (between the incipient outer and lateral sepals) counterclockwise. These histograms were then 4°-binned and used for plotting mean ± SD and kymographs. Total signal was calculated by summing all the bins.

Quantification of developmental robustness

For variability in sepal primordium position, within each bud, an angle was measured between each pair of adjacent sepal primordia with respect to the bud center. CV was calculated within each bud as a measurement of how evenly sepal primordia are distributed around the bud.

For relative initiation timing of sepals within each bud, we considered that the robust temporal sepal initiation pattern in WT consists of the inner sepal initiating within 6 hours of the outer sepal, and the lateral sepal initiating within 12 hours of the outer sepal[16]. Severely delated inner and lateral sepal initiation indicate loss of robustness. Thus, for each genotype, we calculated, among all buds, the mean and SD of initiation timing difference between inner and outer sepals, and between lateral and outer sepals. Robustness is considered lost if sepal initiation does not follow the WT temporal pattern (mean is greater than 6 and 12 respectively), and also if different buds have different temporal patterns (SD is large).

For sepal initiation timing relative to bud size, bud area (μm^2) in maximum intensity projection images were measured in ImageJ[57,58] and used as a proxy for bud size. Representative

378 images of WT vs. *cuc1* (both carrying 35S::mCitrine-RCI2A, a plasma membrane marker) that
379 are of similar area and growth rate throughout the time series were shown. Similarly for WT vs.
380 *5mCUC1*, although they did not have a membrane marker and thus the Chlorophyll channel was
381 used for area measurement. Bud size at the time of outer, inner, and lateral (WT vs *cuc1*) sepal
382 initiation was plotted. For *5mCUC1*, not enough samples initiated lateral sepals, and thus bud
383 size at the time of lateral sepal initiation was not analyzed. We reasoned that buds whose sepals
384 initiate rapidly should be smaller when they initiate sepals, compared to buds whose sepals take
385 longer to initiate. To control for the gradual reduction in size of successive buds during prolonged
386 *in vitro* culture, only buds that did not have any sepals at the first time point and produced at least
387 one sepal at or before the fourth time point (within 18 hours of the first time point) are analyzed.
388

389 ***In vitro* drug treatments on inflorescence samples**

390 For BAP treatment in Fig. 5, inflorescences were dissected, put onto an inflorescence
391 culture medium (see above) containing 0.05% DMSO and 1 μM BAP (6-Benzylaminopurine, Alfa
392 Aesar, A14678). Mock contained just 0.05% DMSO. They were left in a growth chamber for 32
393 hours and then transferred onto inflorescence culture medium without treatments, and imaged at
394 0 h, 24 h, 48 h, and 72 h after the transfer. For BAP treatment in Supplementary Fig. 7e,
395 inflorescences were cultured on media containing 0.01% DMSO and 5 μM BAP (mock contained
396 just 0.01% DMSO) for 96 h, and PI-stained and imaged.

397 For L-Kyn treatment, inflorescences were dissected and put onto an inflorescence culture
398 medium containing 0.02% DMSO and 80 μM L-Kyn (l-kynurenine, Sigma, K8625). Mock
399 contained just 0.02% DMSO. They were left in a growth chamber for 4 days before imaging.

400 For NPA and NPA+NAA treatment, inflorescences were dissected and put onto
401 inflorescence culture medium. The following solutions were made in water: for mock, 0.05%
402 DMSO, 0.01% Silwet L-77; for NPA, 100 μM NPA (Naptalam, Sigma, 33371), 0.05% DMSO,
403 0.01% Silwet L-77; for NPA+NAA, 100 μM NPA, 20 μM NAA (1-Naphthaleneacetic acid, Sigma,

404 N0640), 0.05% DMSO, 0.01% Silwet L-77. These solutions were applied on top of the dissected
405 inflorescences for 24 hours. Then, the solutions were discarded, and samples were washed three
406 times with sterile water. Images were taken 48 hours (for *DR5::3xVENUS-N7*) or 72 hours (for
407 *pCUC1::3xVENUS-N7*) after the end of the treatment.
408

409 **Mass-spring model of a growing floral meristem**

410 We modeled the stage 2 floral meristem as a 2D disk of growing and dividing cells. The
411 simulation begins as a round disk of 73 cells and 348 walls with no auxin, no CUC1, and apolar
412 PIN. As detailed below, in each iteration, the following processes are run in order: deformation of
413 cell walls under turgor pressure (repeated until convergence); dilution of auxin and CUC due to
414 changes in cell size; updating noise in auxin production; 10 steps of chemical interactions; cell
415 division; splitting of cell walls longer than 1 μm; cell growth; reinitialization; data output. The result
416 of each iteration was used as the starting point of the next. Simulations were run for the desired
417 number of iterations. Screenshots and data were saved every 10 iterations.

418 For tissue mechanics, a mass-spring model was used. Cell walls are subdivided to have
419 a maximum length of 1 μm. Wall segments are represented by springs in the simulation, with an
420 initial resting length the same as in the starting configuration. Uniform turgor pressure is simulated
421 by assigning a normal force to the boundary walls, as it cancels out on interior walls. The force
422 acting on a vertex v due to the springs was calculated as:

423 $$F_v = \sum_{n \in N_v} k \left(\frac{\|p_n - p_v\|}{L_{v:n}} - 1 \right) \frac{p_n - p_v}{\|p_n - p_v\|}$$

424 where N_v are neighboring vertices of vertex v, p_v is the position of vertex v, p_n is the position of a
425 neighboring vertex n, k is the spring constant (stiffness), and $L_{v:n}$ is the resting length of the spring
426 joining v and n[59,60]. Stiffness is set uniform and constant for all the cell walls. The resulting system
427 of equations is solved using the backward Euler method with the GPU based stabilized bi-

conjugate gradient solver available in MorphoDynamX. Growth was simulated by increasing the rest length of the springs based on their relative stretch, multiplied by an extensibility factor g:

$$\frac{dL_{v:n}}{dt} = g\left(\frac{\|p_n - p_v\| - L_{v:n}}{L_{v:n}}\right)$$

Within each simulation, extensibility were set constant and uniform for all cell walls. Extensibility was changed when modeling meristems with increased or decreased growth rate.

The molecular interactions are that (1) auxin represses CUC1 expression, and (2) CUC1 increases the sensitivity of PIN repolarization to auxin concentration differences among neighboring cells. To simulate them, each cell is assigned two fields, auxin concentration (aux) and CUC concentration (cuc). Each wall segment is assigned two fields, pin_P and pin_N, denoting the amount of PIN protein on each side that mediates polar auxin transport in either direction. At each chemical step, three calculations take place concomitantly:

(a) For each cell i at time step t, the amount of PIN on its wall facing neighboring cell j is calculated as:

$$pin_{i\to j}(t) = (1-\alpha)pin_{i\to j}(t-1) + \alpha\frac{aux_j^n L_j}{\sum_{k\in N_i} aux_k^n L_k}$$

$$pin_{i\to j}(0) = \frac{L_j}{\sum_{k\in N_i} L_k}$$

where $\alpha = 0.01$ is the PIN repolarization speed, N_i is all the neighboring cells of cell i, L_j and L_k are lengths of cell walls of cell i facing neighboring cells j and k respectively, and aux_j and aux_k are the auxin concentrations of cell j and k respectively. n is the PIN sensitivity factor dependent on the CUC concentration of cell i, cuc_i, and the threshold CUC concentration, $cuc_{thres} = 2$:

$$n = \begin{cases} 1\ (cuc_i < cuc_{thres}) \\ 2\ (cuc_i > cuc_{thres}) \end{cases}$$

Note that the total amount of PIN in each cell sums to 1 over all its cell walls, unaffected by auxin concentration. Also note that a zero-flux boundary condition was used, i.e., no PIN is polarized towards the boundary of the modeled tissue, and there is no flux of auxin across the boundary.

(b) Change in auxin concentration in cell i due to production, decay, and transport

$$\frac{d(aux_i)}{dt} = Prod_{aux} \times \delta_{aux,i} - Dec_{aux} \times aux_i + \frac{Tran_{aux} \sum_{j \in N_i} (aux_j \times pin_{j \to i} - aux_i \times pin_{i \to j})}{Area_i}$$

where $Prod_{aux} = 1$ is the auxin production coefficient, $Dec_{aux} = 0.2$ is the auxin decay coefficient, $Tran_{aux} = 400$ is the polar auxin transport coefficient, N_i are the neighboring cells of i, $Area_i$ is the area of cell i, $pin_{i \to j}$ is the amount of PIN on the wall of cell i facing neighbor j, and $pin_{j \to i}$ is the amount of PIN on the wall of neighbor j facing cell i. $\delta_{aux,i}$ is the auxin production noise of cell i, drawn during initialization and at each iteration from a Gaussian distribution $N(1, SD_{aux})$ where $SD_{aux} = 0.1$ for WT and *cuc1*, and $SD_{aux} = 1$ for *drmy1* and *drmy1 cuc1*, and negative values are set to 0. If the noise is set temporally unchanging (Supplementary Fig. 7), δ_{aux} values are drawn only during initialization but not at each iteration.

(c) Change in CUC concentration in cell i due to production and decay

$$\frac{d(cuc_i)}{dt} = Prod_{cuc} \times \frac{1}{1 + (\frac{aux_i}{K_{aux}})^{hill}} - Dec_{cuc} \times cuc_i$$

where $Prod_{cuc}$ is the CUC production coefficient (1 for WT and *drmy1*, and 0 for *cuc1* and *drmy1 cuc1*), $Dec_{cuc} = 0.2$ is the CUC decay coefficient, $K_{aux} = 5$ is the concentration of auxin at which CUC production is halved, and $hill = 4$ is an arbitrary Hill coefficient.

For cell division, a cell divides when its area passes a threshold of 50 μm^2. Position of the new wall follows the minimal wall length principle, with noise parameters as follows (constant for all simulations): cell division noise 2.0, cell center noise 2.0, wall junction noise 2.0. Daughter cells inherit the same aux, cuc, and δ_{aux}. Split cell walls inherit pin_P and pin_N proportional to their new lengths. New cell walls are assigned infinitesimal (non-zero) starting values of pin_P and pin_N.

Software

Image processing was done in ImageJ (version 2.14.0/1.54f, build c89e8500e4)[57,58] and MorphoGraphX (version 2.0, revision 1-354, CUDA version 11.40)[56]. Modeling was implemented

475 in C++ using vlab (version 5.0, build #3609)[61] and MorphoDynamX (version 2.0, revision 2-1395,
476 CUDA version 11.40; www.MorphoDynamX.org) in an Ubuntu 20.04.6 LTS system, equipped with
477 an Intel Core i9-10900X 3.7 GHz 10-Core Processor, G.Skill Trident Z RGB 256 GB DDR4-3600
478 CL18 Memory, and a NVIDIA GeForce RTX 4090 24 GB Graphics Card. Data processing was
479 done in RStudio (R version 4.3.1 (2023-06-16) -- "Beagle Scouts")[62]. Graphs were made using
480 the package ggplot2 (version 3.4.2)[63]. Fisher's contingency table tests were done using
481 fisher.test. Wilcoxon rank sum tests were done using wilcox.test. Levene's tests of
482 homoscedasticity were done using leveneTest in package "car" (version 3.1-2). Data fitting with
483 ANOVA was done using the function aov. Figures were assembled in Adobe Illustrator (version
484 27.8.1). An RGB color profile "Image P3" was used for all the figures.
485
486 **Statistical analysis**
487 In most cases, each bud, either from the same inflorescence, a different inflorescence
488 from the same plant, or a different plant, is considered a biological replicate. For RNA-seq
489 presented in Fig. 1c, each RNA sample from 5-10 inflorescences of *ap1 cal AP1-GR* background
490 (either WT or *drmy1*), extracted separately, is considered a biological replicate.
491 For bar plots of sepal primordium number or auxin maxima number, all buds (or
492 simulations) were groups by genotype, and then grouped by number, and plotted as stacked bars.
493 For bar-and-whisker plots in Fig. 1c, 4b, 6h, Supplementary Fig. 4c, 4h, bar shows mean, and
494 whiskers show mean ± SD. For violin plots in Fig. 2e, 2k, Supplementary Fig. 3h, 3n, horizontal
495 lines show the quartiles. For circular histograms in Fig. 4d and 5g, lines show mean, and shaded
496 area shows mean ± SD.
497 Student's t-tests in Fig. 4b and Wilcoxon's rank sum tests in Fig. 2e, 2k, Supplementary
498 Fig. 3h, 3n, 4c, 4h are two-tailed, and compare only the indicated pairs of genotypes. For Levene's
499 test of variability in Supplementary Fig. 4c, 4h, center of each group were calculated as mean.
500 For ANOVA, formulae, degree of freedom, F, and p values are indicated in the Figure legends.

For Tukey's HSD in Fig. 6h, 6i, Supplementary Fig. 6d, 7d, all groups (combinations of genotype and growth rate) were fit using a linear model, Estimated Marginal Means (EMM) were calculated, and significant differences were indicated using compact letter display.

For RNA-seq, an FDR of 0.05 was used. For Tukey's HSD, family-wise type I error rate was 0.05. For all other analyses, a p-value threshold of 0.05 was used.

Data availability

Data behind all the graph quantifications are available in Supplementary Dataset 1. RNA seq data are available in GEO under project number PRJNA957462 and dataset number GSE230100.

Code availability

Source code for the computational model, a tutorial, and demo data are available in Supplementary Dataset 2 and also on GitHub (https://github.com/RoederLab/MassSpringAuxin).

516 **REFERENCES**

517 1. Araújo, I. S. *et al.* Stochastic gene expression in *Arabidopsis thaliana*. *Nat. Commun.* **8**,
518 2132 (2017).
519 2. Hong, L. *et al.* Variable Cell Growth Yields Reproducible Organ Development through
520 Spatiotemporal Averaging. *Dev. Cell* **38**, 15–32 (2016).
521 3. Le Gloanec, C. *et al.* Cell type-specific dynamics underlie cellular growth variability in
522 plants. *Dev.* **149**, dev200783 (2022).
523 4. Lachowiec, J., Queitsch, C. & Kliebenstein, D. J. Molecular mechanisms governing
524 differential robustness of development and environmental responses in plants. *Ann. Bot.*
525 **117**, 795–809 (2016).
526 5. Roeder, A. H. K. *et al.* Fifteen compelling open questions in plant cell biology. *Plant Cell*
527 **34**, 72–102 (2022).
528 6. Hintze, M., Katsanos, D., Shahrezaei, V. & Barkoulas, M. Phenotypic Robustness of
529 Epidermal Stem Cell Number in *C. elegans* Is Modulated by the Activity of the Conserved
530 N-acetyltransferase nath-10/NAT10. *Front. Cell Dev. Biol.* **9**, 640856 (2021).
531 7. Garelli, A., Gontijo, A. M., Miguela, V., Caparros, E. & Dominguez, M. Imaginal discs
532 secrete insulin-like peptide 8 to mediate plasticity of growth and maturation. *Science* **336**,
533 579–582 (2012).
534 8. Folta, A. *et al.* Over-expression of Arabidopsis AtCHR23 chromatin remodeling ATPase
535 results in increased variability of growth and gene expression. *BMC Plant Biol.* **14**, 76
536 (2014).
537 9. Cassidy, J. J. *et al.* MiR-9a minimizes the phenotypic impact of genomic diversity by
538 buffering a transcription factor. *Cell* **155**, 1556–1567 (2013).
539 10. Maugarny, A. *et al.* Compensation of compromised PRC2 regulation by a miRNA ensures
540 robustness of Arabidopsis leaf development. *Preprint at bioRxiv:*
541 https://doi.org/10.1101/2023.10.11.561475 (2023).

11. Tsai, T. Y. C. *et al.* An adhesion code ensures robust pattern formation during tissue morphogenesis. *Science* **370**, 113–116 (2020).

12. Besnard, F. *et al.* Cytokinin signalling inhibitory fields provide robustness to phyllotaxis. *Nature* **505**, 417–421 (2014).

13. Li, P. *et al.* Morphogen gradient reconstitution reveals Hedgehog pathway design principles. *Science* **360**, 543–548 (2018).

14. Winter, K. U. *et al.* Evolution of class B floral homeotic proteins: Obligate heterodimerization originated from homodimerization. *Mol. Biol. Evol.* **19**, 587–596 (2002).

15. Xiong, F. *et al.* Specified neural progenitors sort to form sharp domains after noisy Shh signaling. *Cell* **153**, 550–561 (2013).

16. Zhu, M. *et al.* Robust organ size requires robust timing of initiation orchestrated by focused auxin and cytokinin signalling. *Nat. Plants* **6**, 686–698 (2020).

17. Kong, S. *et al.* DRMY1 promotes robust morphogenesis by sustaining translation of a hormone signaling protein. *Preprint at bioRxiv:* https://doi.org/10.1101/2023.10.11.561475 (2023).

18. Trinh, D.-C. Increased gene expression variability hinders the formation of regional mechanical conflicts leading to reduced organ shape robustness. *Proc. Natl. Acad. Sci.* **120**, 2017 (2023).

19. Lander, A. D., Gokoffski, K. K., Wan, F. Y. M., Nie, Q. & Calof, A. L. Cell lineages and the logic of proliferative control. *PLoS Biol.* **7**, e1000015 (2009).

20. Lander, A. D. Pattern, growth, and control. *Cell* **144**, 955–969 (2011).

21. Li, R., Liu, Y., Pedersen, H. S., Kragh, P. M. & Callesen, H. Development and quality of porcine parthenogenetically activated embryos after removal of zona pellucida. *Theriogenology* **80**, 58–64 (2013).

22. Roeder, A. H. K. Arabidopsis sepals: A model system for the emergent process of morphogenesis. *Quant. Plant Biol.* **2**, e14 (2021).

568 23. Olsen, A. N., Ernst, H. A., Leggio, L. Lo & Skriver, K. NAC transcription factors: Structurally
569 distinct, functionally diverse. *Trends Plant Sci.* **10**, 79–87 (2005).
570 24. Aida, M. & Tasaka, M. Genetic control of shoot organ boundaries. *Curr. Opin. Plant Biol.*
571 **9**, 72–77 (2006).
572 25. Bilsborough, G. D. *et al.* Model for the regulation of *Arabidopsis thaliana* leaf margin
573 development. *Proc. Natl. Acad. Sci. U. S. A.* **108**, 3424–3429 (2011).
574 26. Furutani, M. *et al.* PIN-FORMED1 and PINOID regulate boundary formation and cotyledon
575 development in Arabidopsis embryogenesis. *Development* **131**, 5021–5030 (2004).
576 27. Aida, M., Vernoux, T., Furutani, M., Traas, J. & Tasaka, M. Roles of PIN-FORMED1 and
577 MONOPTEROS in pattern formation of the apical region of the Arabidopsis embryo.
578 *Development* **129**, 3965–3974 (2002).
579 28. Mallory, A. C., Dugas, D. V., Bartel, D. P. & Bartel, B. MicroRNA regulation of NAC-domain
580 targets is required for proper formation and separation of adjacent embryonic, vegetative,
581 and floral organs. *Curr. Biol.* **14**, 1035–1046 (2004).
582 29. Sieber, P., Wellmer, F., Gheyselinck, J., Riechmann, J. L. & Meyerowitz, E. M. Redundancy
583 and specialization among plant microRNAs: Role of the MIR164 family in developmental
584 robustness. *Development* **134**, 1051–1060 (2007).
585 30. Baker, C. C., Sieber, P., Wellmer, F. & Meyerowitz, E. M. The early extra petals1 mutant
586 uncovers a role for microRNA miR164c in regulating petal number in Arabidopsis. *Curr.*
587 *Biol.* **15**, 303–315 (2005).
588 31. Aida, M., Ishida, T., Fukaki, H., Fujisawa, H. & Tasaka, M. Genes involved in organ
589 separation in Arabidopsis: An analysis of the *cup-shaped cotyledon* mutant. *Plant Cell* **9**,
590 841–857 (1997).
591 32. Hibara, K. I. *et al.* Arabidopsis CUP-SHAPED COTYLEDON3 regulates postembryonic
592 shoot meristem and organ boundary formation. *Plant Cell* **18**, 2946–2957 (2006).
593 33. Dinneny, J. R., Yadegari, R., Fischer, R. L., Yanofsky, M. F. & Weigel, D. The role of

JAGGED in shaping lateral organs. *Development* **131**, 1101–1110 (2004).

34. Long, J. & Barton, M. K. Initiation of axillary and floral meristems in Arabidopsis. *Dev. Biol.* **218**, 341–353 (2000).

35. Peng, Z. *et al.* Differential growth dynamics control aerial organ geometry. *Curr. Biol.* **32**, 4854-4868.e5 (2022).

36. Ohno, C. K., Reddy, G. V., Heisler, M. G. B. & Meyerowitz, E. M. The Arabidopsis *JAGGED* gene encodes a zinc finger protein that promotes leaf tissue development. *Development* **131**, 1111–1122 (2004).

37. Růzička, K. *et al.* Cytokinin regulates root meristem activity via modulation of the polar auxin transport. *Proc. Natl. Acad. Sci. U. S. A.* **106**, 4284–4289 (2009).

38. Marhavý, P. *et al.* Cytokinin controls polarity of PIN1-dependent Auxin transport during lateral root organogenesis. *Curr. Biol.* **24**, 1031–1037 (2014).

39. Galbiati, F. *et al.* An integrative model of the control of ovule primordia formation. *Plant J.* **76**, 446–455 (2013).

40. Reinhardt, D. *et al.* Regulation of phyllotaxis by polar auxin transport. *Nature* **426**, 255–260 (2003).

41. Smith, R. S. *et al.* A plausible model of phyllotaxis. *Proc. Natl. Acad. Sci. U. S. A.* **103**, 1301–1306 (2006).

42. Jönsson, H., Heisler, M. G., Shapiro, B. E., Meyerowitz, E. M. & Mjolsness, E. An auxin-driven polarized transport model for phyllotaxis. *Proc. Natl. Acad. Sci. U. S. A.* **103**, 1633–1638 (2006).

43. Gregor, T., Tank, D. W., Wieschaus, E. F. & Bialek, W. Probing the Limits to Positional Information. *Cell* **130**, 153–164 (2007).

44. Erdmann, T., Howard, M. & Ten Wolde, P. R. Role of spatial averaging in the precision of gene expression patterns. *Phys. Rev. Lett.* **103**, 2–5 (2009).

45. Waddington, C. H. Canalization of Development and the Inheritance of Acquired

620 Characters. *Nature* **150**, 563–656 (1942).

621 46. Friml, J. *et al.* A PINOID-dependent binary switch in apical-basal PIN polar targeting directs
622 auxin efflux. *Science* **306**, 862–865 (2004).

623 47. Zourelidou, M. *et al.* Auxin efflux by PIN-FORMED proteins is activated by two different
624 protein kinases, D6 PROTEIN KINASE and PINOID. *eLife* **3**, e02860 (2014).

625 48. Michniewicz, M. *et al.* Antagonistic Regulation of PIN Phosphorylation by PP2A and
626 PINOID Directs Auxin Flux. *Cell* **130**, 1044–1056 (2007).

627 49. Titapiwatanakun, B. *et al.* ABCB19/PGP19 stabilises PIN1 in membrane microdomains in
628 Arabidopsis. *Plant J.* **57**, 27–44 (2009).

629 50. Nagawa, S. *et al.* ROP GTPase-dependent actin microfilaments promote PIN1 polarization
630 by localized inhibition of clathrin-dependent endocytosis. *PLoS Biol.* **10**, e1001299 (2012).

631 51. Heisler, M. G. *et al.* Alignment between PIN1 polarity and microtubule orientation in the
632 shoot apical meristem reveals a tight coupling between morphogenesis and auxin
633 transport. *PLoS Biol.* **8**, e1000516 (2010).

634 52. Heisler, M. G. *et al.* Patterns of auxin transport and gene expression during primordium
635 development revealed by live imaging of the Arabidopsis inflorescence meristem. *Curr.*
636 *Biol.* **15**, 1899–1911 (2005).

637 53. Gonçalves, B. *et al.* A conserved role for *CUP-SHAPED COTYLEDON* genes during ovule
638 development. *Plant J.* **83**, 732–742 (2015).

639 54. Marin, E. *et al.* mir390, Arabidopsis TAS3 tasiRNAs, and their AUXIN RESPONSE
640 FACTOR targets define an autoregulatory network quantitatively regulating lateral root
641 growth. *Plant Cell* **22**, 1104–1117 (2010).

642 55. Smyth, D. R., Bowman, J. L. & Meyerowitz, E. M. Early flower development in Arabidopsis.
643 *Plant Cell* **2**, 755–767 (1990).

644 56. Strauss, S. *et al.* Using positional information to provide context for biological image
645 analysis with MorphoGraphX 2.0. *eLife* **11**, e72601 (2022).

57. Schindelin, J. *et al.* Fiji: An open-source platform for biological-image analysis. *Nat. Methods* **9**, 676–682 (2012).

58. Schindelin, J., Rueden, C. T., Hiner, M. C. & Eliceiri, K. W. The ImageJ ecosystem: An open platform for biomedical image analysis. *Mol. Reprod. Dev.* **82**, 518–529 (2015).

59. Majda, M. *et al.* Elongation of wood fibers combines features of diffuse and tip growth. *New Phytol.* **232**, 673–691 (2021).

60. Mosca, G. *et al.* Modeling Plant Tissue Growth and Cell Division. in *Mathematical Modelling in Plant Biology* 107–138 (2018). doi:10.1007/978-3-319-99070-5_7.

61. Federl & Prusinkiewicz. Virtual laboratory: an interactive software environment for computer graphics. in *1999 Proceedings Computer Graphics International* 93–100 (1999). doi:10.1109/CGI.1999.777921.

62. R Core Team (2021). R: A language and environment for statistical computing. R Foundation for Statistical Computing, Vienna, Austria. URL https://www.R-project.org/.

63. Wickham, H. *ggplot2: Elegant Graphics for Data Analysis*. (Springer, 2009). doi:10.1007/978-0-387-98141-3.

662 **ACKNOWLEDGEMENTS**

663 We thank Isabella Burda, Trevor Cross, Michelle Heeney, Henrik Jönsson, Byron Rusnak, and
664 Avilash Singh Yadav for comments and suggestions on the manuscript. We thank Elliot
665 Meyerowitz and Arnavaz Garda for the *DR5::3xVENUS-N7*/*PIN1::GFP* (Ler) seeds and the
666 *pCUC1::3xVENUS-N7* construct. We thank Mitsuhiro Aida for the *pCUC1::CUC1-GFP* seeds. We
667 thank Alexis Maizel for the *DR5::ER-mRFP1.2* seeds. We thank Arabidopsis Biological Resource
668 Center for providing seeds used in this research. We thank Addgene for providing the *5mCUC1*
669 *pGreenII0129* construct (#12067). Research reported in this publication was supported by the
670 National Institute of General Medical Sciences of the National Institutes of Health (NIH) under
671 award number R01GM134037 to A.H.K.R., and a Biotechnological and Biological Sciences
672 Research Council (BBSRC) Institute Strategic Program Grant (BB/X01102X/1) to R.S.S. The
673 content is solely the responsibility of the authors and does not necessarily represent the official
674 views of the National Institutes of Health.

675

676 **AUTHOR CONTRIBUTIONS**

677 Conceptualization and design of experiments were done by S.K., M.Z., and A.H.K.R. Experiments
678 were carried out by S.K. Data analysis was done by S.K. and D.P. The MorphoDynamX modeling
679 platform was developed by B.L. and R.S.S. The floral meristem model was developed by S.K.
680 based on scripts written by B.L. and R.S.S. Manuscript was prepared by S.K. and edited by all
681 the authors. Funds were provided by A.H.K.R. and R.S.

682

683 **COMPETING INTERESTS**

684 The authors declare no competing interests.

685

686 **MATERIALS AND CORRESPONDENCE**

687 Material requests and correspondence should be addressed to A.H.K.R.

FIGURES

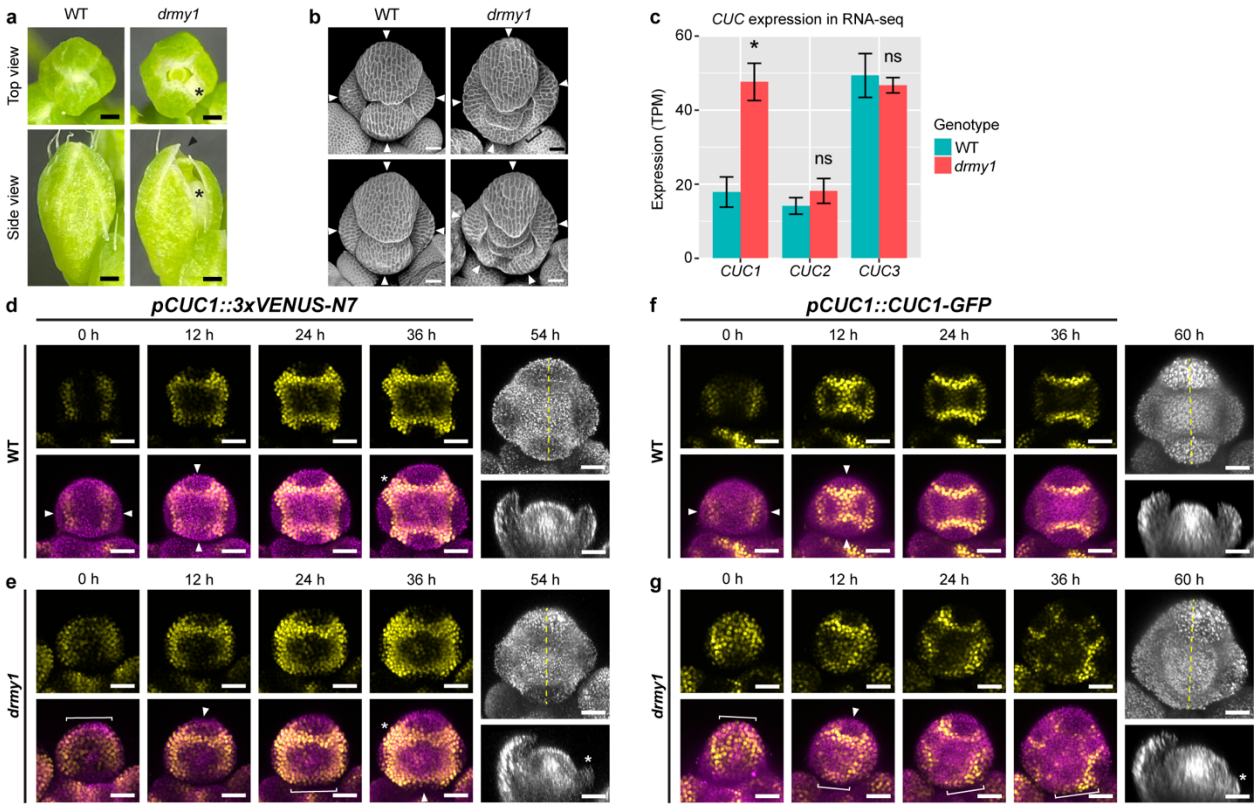

Fig. 1. CUC1 is upregulated in *drmy1* with disrupted spatial pattern.

(a-b) Floral phenotype of the *drmy1* mutant. **(a)** Stage 12 buds of WT (left) and *drmy1* (right). In *drmy1*, asterisk indicates a gap on the side due to uneven sepal positions; arrowhead indicates a gap on the top caused by unequal sepal length. Scale bars, 250 µm. **(b)** Two stage 6 buds of WT (left), and two *drmy1* buds with matching outer sepal size. Arrowheads point to sepal primordia. Note that sepal primordia in *drmy1* are of variable size, number, and position, leaving regions in the bud periphery with no sepal outgrowth (bracket). Scale bars, 25 µm.

(c) Expression of *CUC* genes in floral tissue of WT vs *drmy1* (in Ler *ap1 cal AP1-GR* background), as determined by RNA-seq. n = 3 samples per genotype. Adjusted p-values from DESeq2: CUC1, 3.710×10^{-13}; CUC2, 0.6650; CUC3, 0.2292. Complete dataset is in Kong et al. (2023)[17].

(d-e) Expression pattern of *CUC1* in WT **(d)** and *drmy1* **(e)**, live imaged through time. For 0 to 36 hours, top row shows *pCUC1::3xVENUS-N7*, and bottom row shows *pCUC1::3xVENUS-N7*

(yellow) merged with Chlorophyll (magenta; to show flower morphology). For 54 hours, the chlorophyll channel and its longitudinal section (dashed lines) are shown. Note that in WT, four boundaries with high *CUC1* expression form at robust positions between the incipient sepal primordia and the center of the floral meristem at stage 2 (arrowheads), corresponding to the robust initiation of four sepals at stage 3. In *drmy1*, *CUC1* expression expands to the bud periphery (brackets). Although this peripheral expression later narrows to boundary domains (arrowheads), it correlates with limited sepal outgrowth at stage 3 (asterisk). *CUC1* expression in the inter-sepal regions are also expanded in *drmy1* (asterisks). See Supplementary Movie 1. Images are representative of n = 4 WT buds and n = 5 *drmy1* buds. Note that plants are heterozygous for *pCUC1::3xVENUS-N7*. Scale bars, 25 µm.

(f-g) Protein accumulation pattern of CUC1 in WT **(f)** and *drmy1* **(g)**, live imaged through time. For 0 to 36 hours, top row shows *pCUC1::CUC1-GFP*, and bottom row shows *pCUC1::CUC1-GFP* (yellow) merged with Chlorophyll (magenta). For 60 hours, the chlorophyll channel and its longitudinal section (dashed lines) are shown. Note that in WT, four boundaries with high CUC1 protein accumulation form at robust positions between the incipient primordia and the center of the floral meristem at stage 2 (arrowheads), corresponding to the robust initiation of four sepals at stage 3. In *drmy1*, CUC1 protein accumulation is initially much higher and less boundary-restricted, and often in the bud periphery (brackets). In some regions, CUC1 accumulation narrows to boundary domains (arrowheads), while in other regions, it remains in the bud periphery, correlated with limited sepal outgrowth at stage 3 (asterisk). See Supplementary Movie 2. Images are representative of n = 2 WT buds and n = 4 *drmy1* buds. Scale bars, 25 µm.

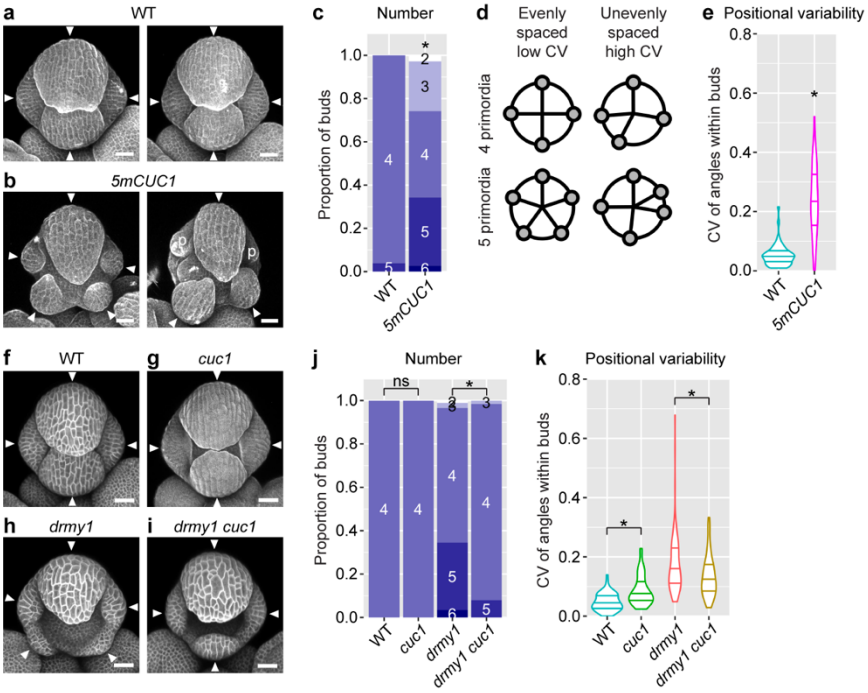

Fig. 2. *CUC1* upregulation is sufficient and necessary for variable sepal initiation

(a-e) *CUC1* upregulation causes variable sepal initiation. **(a-b)** Two representative WT **(a)** and *5mCUC1* **(b)** buds stained with PI. Arrowheads show sepal primordia. "p" shows petal primordia. Scale bars, 25 µm. **(c)** Quantification of sepal primordium number in each bud, color-coded by number and grouped by genotype. **(d)** Illustration of quantifying variability in sepal position. Buds in which sepal primordia are evenly distributed around the bud have low CV values of angular distanced between adjacent sepal primordia (left). Buds in which sepal primordia are irregularly positioned have high CV values of angles between adjacent sepals (right). Reproduced from Kong et al. (2023)[17]. **(e)** Quantification of positional variability in WT vs *5mCUC1*. Sample size: WT, n = 51 buds; *5mCUC1*, n = 70 buds. Asterisks indicate statistically significant differences from WT in a Fisher's contingency table test ($p = 4.535\times10^{-14}$) **(c)** or Wilcoxon rank sum test ($p = 2.878\times10^{-16}$) **(e)**.

(f-k) The *cuc1* mutation rescues variability in sepal number and position in *drmy1*. **(f-i)** Representative buds of WT **(f)**, *cuc1* **(g)**, *drmy1* **(h)**, and *drmy1 cuc1* **(i)**. The *cuc1* bud was PI-

740 stained, and others carried the *35S::mCitrine-RCI2A* membrane marker. Arrowheads point to
741 sepal primordia. Scale bars, 25 μm. **(j-k)** Quantification of sepal primordium number **(j)** and
742 positional variability **(k)** as described above. Sample size: WT, n = 66 buds; *cuc1*, n = 52 buds;
743 *drmy1*, n = 87 buds; *drmy1 cuc1*, n = 63 buds. Asterisks indicate statistically significant differences
744 in a Fisher's contingency table test **(j)** or Wilcoxon rank sum test **(k)**, and ns means no significant
745 differences. P-values for **(j)**: WT vs. *cuc1*, p = 1; *drmy1* vs. *drmy1 cuc1*, p = 2.575×10^{-4}. P-values
746 for **(k)**: WT vs. *cuc1*, p = 2.665×10^{-6}; *drmy1* vs. *drmy1 cuc1*, p = 4.922×10^{-3}.

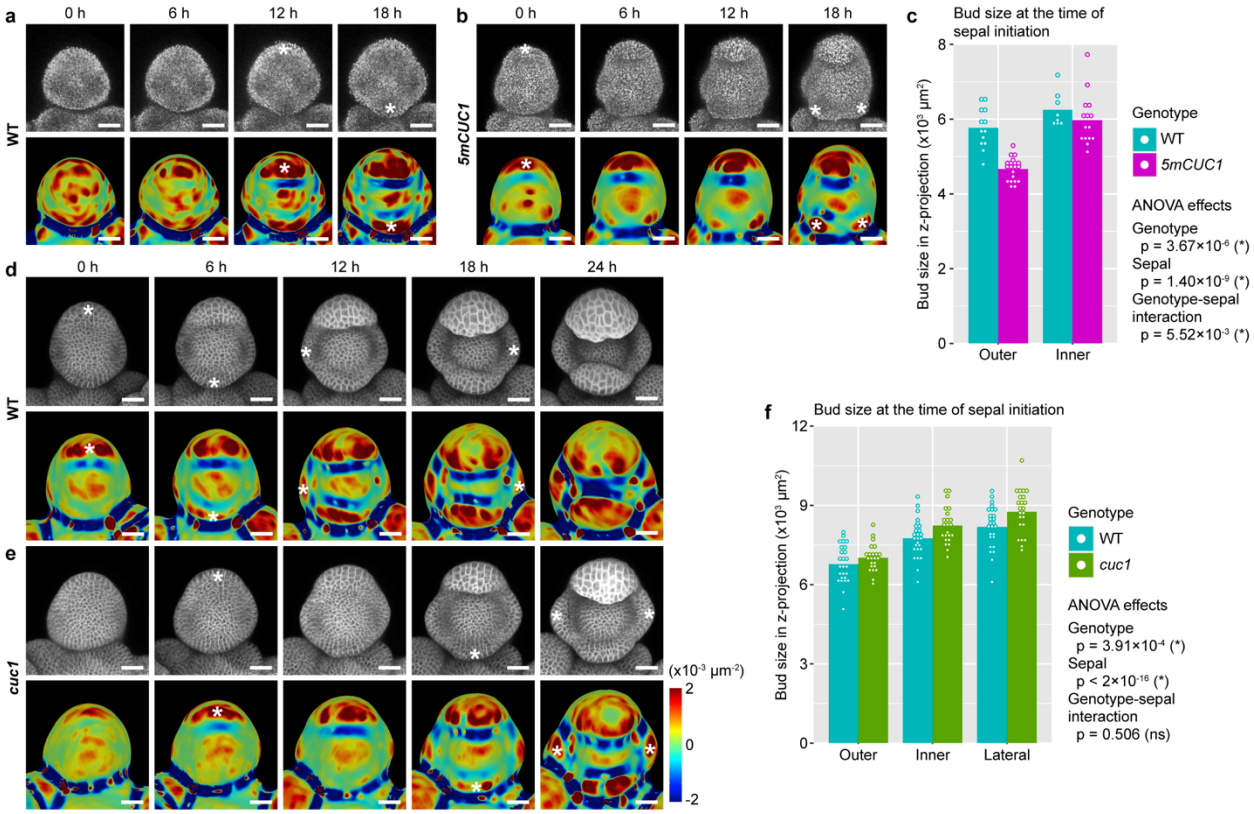

Fig. 3. CUC1 promotes rapid sepal initiation.

(a-c) The outer sepal initiates more rapidly in *5mCUC1* than WT. **(a,b)** show one bud of WT **(a)** and one bud of *5mCUC1* **(b)** live imaged every 6 hours for 18 hours. Chlorophyll channel is shown on the top, and Gaussian curvature of extracted surfaces is on the bottom. The buds were matched for size, indicating matched developmental stage. Asterisks indicate sepal initiation events. Note that outer sepal initiation was much earlier in *5mCUC1* than WT. **(c)** Quantification of bud size (area in Z-projections; as a proxy for developmental stage) at the time of sepal initiation. Shown are mean (bars) and individual buds (dots). Sample size, WT outer sepal, n = 13; *5mCUC1* outer sepal, n = 20; WT inner sepal, n = 8; *5mCUC1* inner sepal, n = 15. An ANOVA model of Size ~ Genotype * Sepal was fit. Genotype, degree of freedom (df) = 1, F = 26.823, p = 3.67×10^{-6}. Sepal, df = 1, F = 53.946, p = 1.40×10^{-9}. Interaction, df = 1, F = 8.387, p = 5.52×10^{-3}. **(d-f)** Sepals initiate more slowly in *cuc1* than WT. **(d,e)** show one bud of WT **(d)** and one bud of *cuc1* **(e)** live imaged every 6 hours for 24 hours. Chlorophyll is shown on the top, and Gaussian

curvature of extracted surfaces is on the bottom. The buds were matched for size, indicating matched developmental stage. Asterisks indicate sepal initiation events. Note that overall sepal initiation is delayed in *cuc1* compared to WT. **(f)** Quantification of bud size (area in Z-projections; as a proxy for developmental stage) at the time of sepal initiation. Shown are mean (bars) and individual buds (dots). Sample size, 26 buds for WT and 23 buds for *cuc1*. An ANOVA model of Size ~ Genotype * Sepal was fit. Genotype, df = 1, F = 13.198, $p = 3.91\times10^{-4}$. Sepal, df = 2, F = 60.760, $p < 2\times10^{-16}$. Interaction, df = 2, F = 0.685, p = 0.5055. Scale bar in all images, 25 μm.

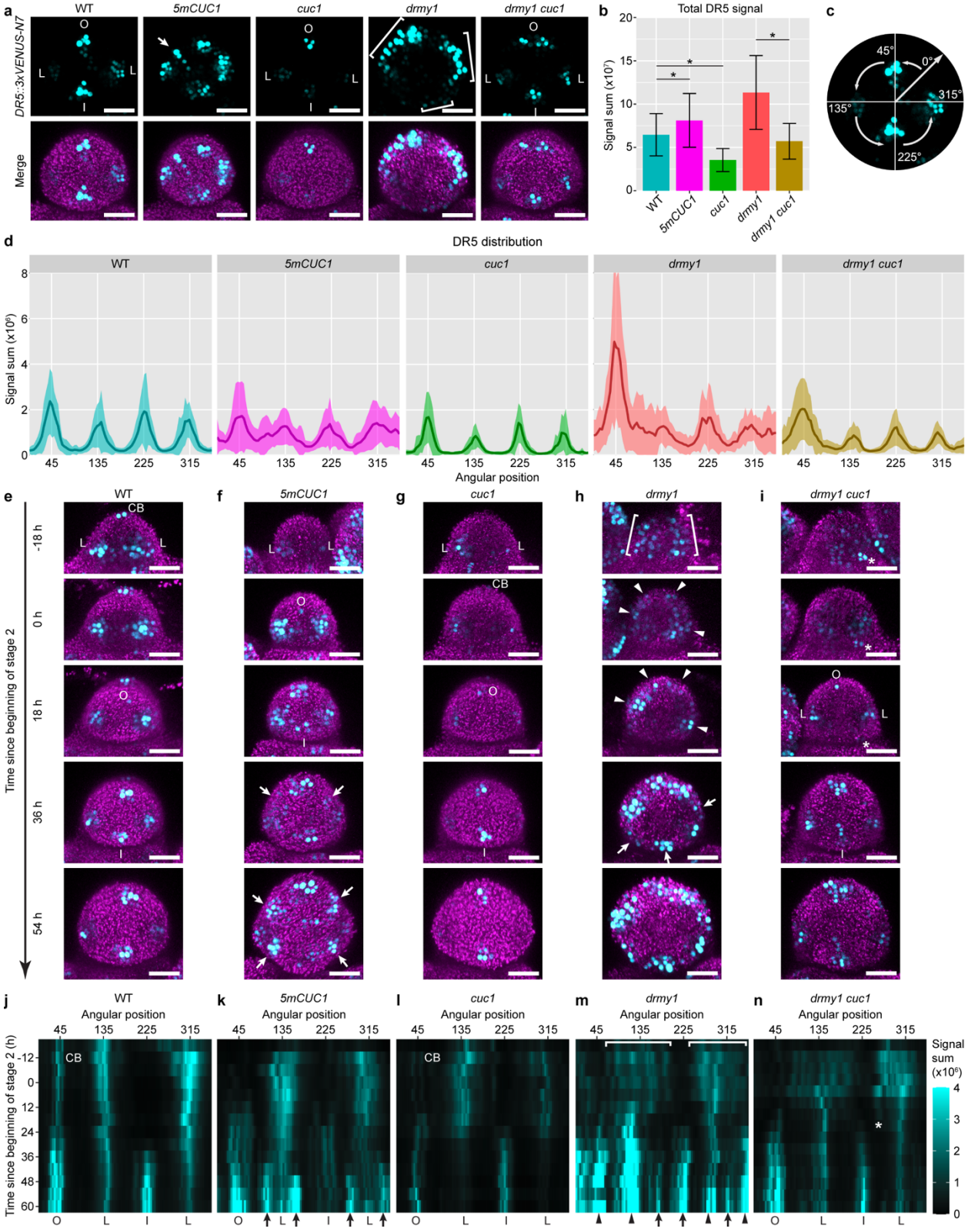
a
WT
5mCUC1
cuc1
drmy1
drmy1 cuc1
DR5::3xVENUS-N7
Merge
b
Total DR5 signal
Signal sum (x10⁷)
c
45°
0°
315°
135°
225°
d
DR5 distribution
Signal sum (x10⁶)
Angular position
e
f
g
h
i
Time since beginning of stage 2
-18 h
0 h
18 h
36 h
54 h
j
k
l
m
n
Angular position
Time since beginning of stage 2 (h)
Signal sum (x10⁶)

768

Fig. 4. CUC1 overexpression is necessary and sufficient for variability in auxin maxima patterning

(a-d) Auxin patterning is disrupted in *5mCUC1* and *drmy1* but rescued in *drmy1 cuc1*. **(a)** Representative images of *DR5::3xVENUS-N7* (cyan, top row) and DR5 merged with the chlorophyll channel (magenta, bottom row) in stage 2 buds of WT, *5mCUC1*, *cuc1*, *drmy1*, and *drmy1 cuc1*. **(b)** Quantification of total DR5 signal (mean ± SD). Asterisks indicate statistically significant differences in two-tailed t-tests (WT vs. *5mCUC1*, $p = 0.0266$; WT vs. *cuc1*, $p = 2.09\times10^{-6}$; *drmy1* vs. *drmy1 cuc1*, $p = 1.32\times10^{-6}$). **(c)** Illustration of circular histogram analysis in **(d)** and **(j-n)**. Each bud was aligned so that the incipient outer sepal was on the top and the inflorescence meristem on the bottom. DR5 signal was quantified in 4°-bins around the Z-axis starting between the incipient lateral and outer sepal, so that the incipient outer sepal would be at 45°. **(d)** Circular histograms of DR5 in each genotype showing mean ± SD. Sample size: WT, n = 30 buds; *5mCUC1*, n = 29 buds; *cuc1*, n = 19 buds; *drmy1*, n = 24 buds; *drmy1 cuc1*, n = 32 buds. **(e-n)** *CUC1* upregulation promotes auxin maxima formation, but can amplify sporadic auxin patches. **(e-i)** Live imaging of stage 2 buds of WT, *5mCUC1*, *cuc1*, *drmy1*, and *drmy1 cuc1* carrying *DR5::3xVENUS-N7*. Shown is DR5 (cyan) merged with the chlorophyll channel (magenta). On the left shows time relative to the beginning of stage 2 (second row), an indicator of developmental progression. **(j-n)** Kymographs showing DR5 signal through time, in the same buds as in **(e-i)**. O, incipient outer sepal; I, incipient inner sepal; L, incipient lateral sepal; CB, cryptic bract. Brackets indicate diffuse bands of auxin signaling that later form distinct, variably positioned auxin maxima (arrowheads). Arrows indicate additional auxin maxima that form in the space between existing ones. Asterisks indicate a sporadic auxin patch that gradually disappears in *drmy1 cuc1*. Scale bar in all images, 25 µm.

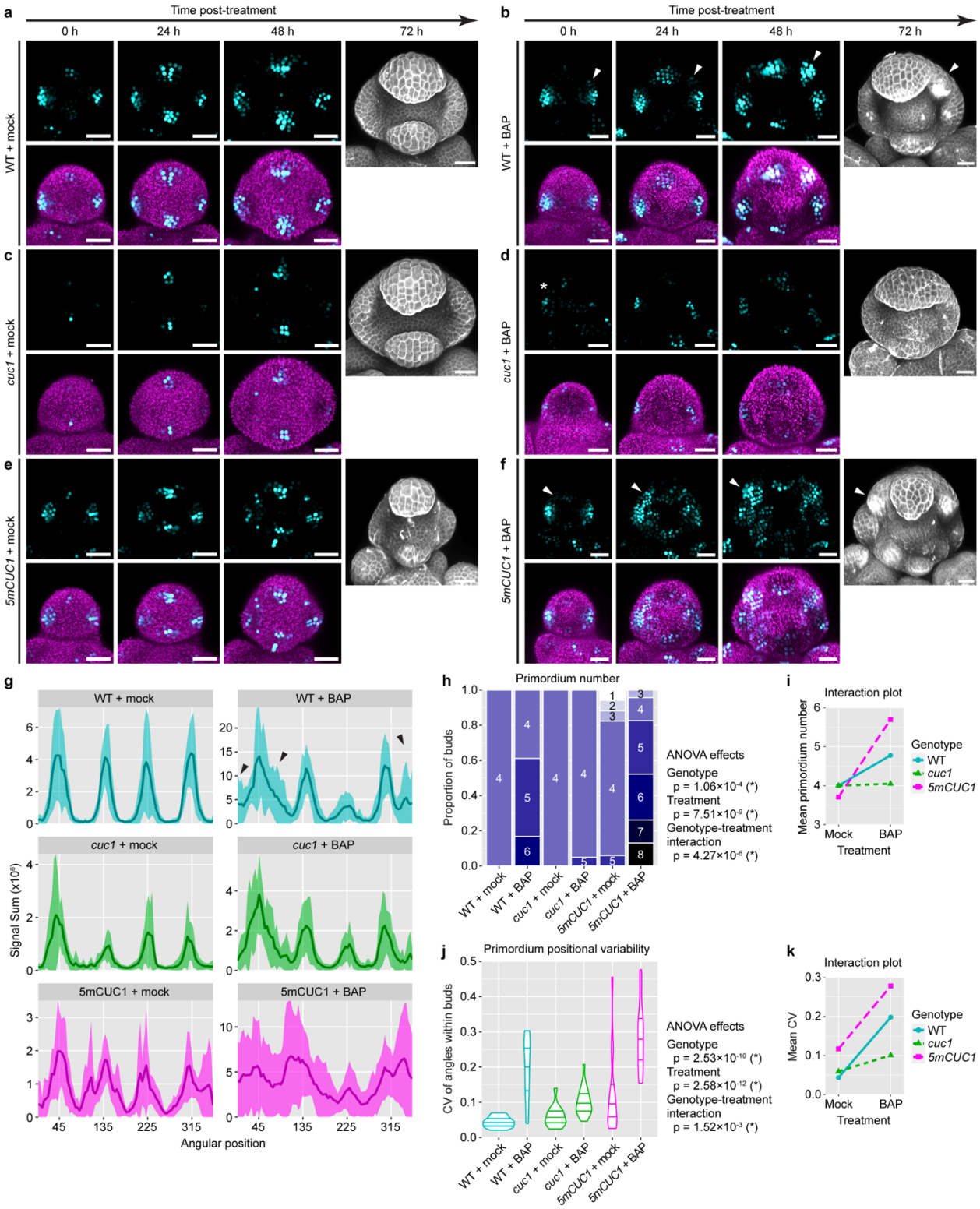

Fig. 5. CUC1 amplifies sporadic auxin patches to form variably positioned auxin maxima and primordia.

(a-f) WT **(a,b)**, *cuc1* **(c,d)**, and *5mCUC1* **(e,f)** were treated with mock (DMSO) **(a,c,e)** or 1 μM BAP **(b,d,f)** for 32 hours and then transferred onto non-treatment media (0 h) and live-imaged every 24 hours for four time points. For 0 h, 24 h, and 48 h, top rows show *DR5::3xVENUS-N7* (cyan) and bottom rows show DR5 merged with the Chlorophyll channel (magenta). For 72 h, buds were PI-stained. Note that BAP treatment disrupts robust auxin patterning and causes sporadic auxin patches. In *cuc1*, sporadic patches disappear (asterisk), whereas in WT and *5mCUC1*, they are amplified to form variably positioned auxin maxima and sepal primordia (arrowheads). Scale bars, 25 μm.

(g) Circular histograms of DR5 in late stage 2 and early stage 3 buds at 48 h post-treatment. Shown is mean ± SD. Note that BAP treatment causes regions of great variability in WT (large SD, black arrows), which is less pronounced in *cuc1* and more pronounced in *5mCUC1*. Sample size: WT + mock, n = 11 buds; WT + BAP, n = 17 buds; *cuc1* + mock, n = 11 buds; *cuc1* + BAP, n = 19 buds; *5mCUC1* + mock, n = 13 buds; *5mCUC1* + BAP, n = 20 buds.

(h-k) Quantification of variability in primordium number **(h,i)** and position **(j,k)** in stage 3 and 4 buds at 72 h post-treatment. **(h)** shows the number of primordia in each bud, grouped by genotype. An ANOVA model of Number ~ Genotype * Treatment was fit. Genotype, df = 2, F = 10.04, $p = 1.06\times10^{-4}$. Treatment, df = 1, F = 39.81, $p = 7.51\times10^{-9}$. Interaction, df = 2, F = 14.01, $p = 4.27\times10^{-6}$. **(j)** shows a violin plot of the CV of angles between adjacent primordia in each bud. An ANOVA model of CV ~ Genotype * Treatment was fit. Genotype, df = 2, F = 27.790, $p = 2.53\times10^{-10}$. Treatment, df = 1, F = 63.585, $p = 2.58\times10^{-12}$. Interaction, df = 2, F = 6.932, $p = 1.52\times10^{-3}$. Note that both sepal and petal primordia were counted, as they were hard to distinguish in many cases. **(i,k)** shows the respective interactions plots of mean primordium number **(i)** and mean CV of position **(k)**. Note that *5mCUC1* further increases the variability caused by BAP treatment, while *cuc1* is largely resistant to the effect of BAP. Sample size: WT + mock, n = 13 buds; WT + BAP, n = 18 buds; *cuc1* + mock, n = 15 buds; *cuc1* + BAP, n = 21 buds; *5mCUC1* + mock, n = 17; *5mCUC1* + BAP, n = 23.

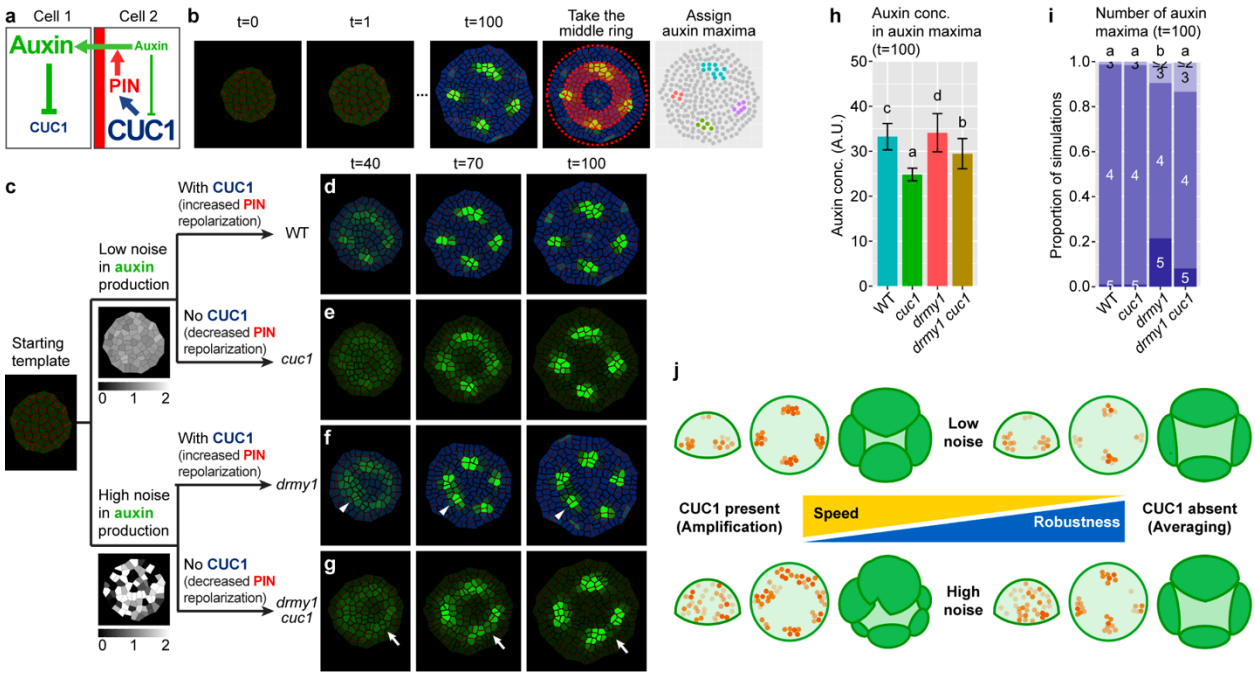

Fig. 6. The noise-amplifying effect of CUC1 can be fully explained by an increase in PIN repolarization.

(a) Diagram of auxin-CUC1 interaction implemented in the model. Auxin represses *CUC1* expression, whereas CUC1 increases PIN repolarization. PIN1 polarizes toward neighboring cells with highest auxin concentration and moves auxin out of the cell into its neighbors. **(b)** Modeling approach. The floral meristem is modeled with a 2D disk of cells, which starts patternless. Molecular interactions in **(a)** generate auxin distribution patterns. Auxin maxima within the shaded middle ring (1/3 < r < 2/3 of total radius) were extracted and quantified. **(c)** How genotypes were modeled. The *drmy1* mutation is modeled as having higher noise in auxin production. The *cuc1* mutation is modeled by removing CUC1 (which decreases PIN1 repolarization). **(d-i)** Removing CUC1 rescues the variability in auxin patterning of *drmy1*. Shown are simulations of WT **(d)**, *cuc1* **(e)**, *drmy1* **(f)**, and *drmy1 cuc1* **(g)**. Note that while a sporadic auxin patch in *drmy1* was amplified to form an auxin maximum (arrowhead), a similar patch in *drmy1 cuc1* dissipates (arrow). Growth rate, 0.8. **(h)** shows simulated auxin concentration averaged across all auxin maxima within each bud (mean ± SD). **(i)** shows the number of auxin maxima in each bud at t=100. Quantifications

were done across n=500 simulations of each genotype. Letters show multiple comparison using Tukey's HSD. **(j)** A tradeoff exists between the speed and robustness of morphogenesis. Having CUC1 promotes rapid morphogenesis under low noise conditions (top left), yet disrupts robustness under high noise conditions such as *drmy1* or BAP treatment (bottom left). Removing CUC1 reduces auxin maxima intensity and sepal initiation speed (top right), but allows additional time for noise to dissipate and robust pattern to form under high noise conditions (bottom right).